RSC Advances

PAPER

View Article Online
View Journal | View Issue



Cite this: *RSC Adv.*, 2024, **14**, 6041

# Preparation of high-performance anti-aging polypropylene by modified nano-$TiO_2$ and calcium sulfate whisker grafted acrylonitrile composite PP†

Shanshan Cong,[ab] Tianyu Lan,[*bcd] Yazhen Wang,[*d] Liwu Zu,[d] Shaobo Dong[d] and Zuoyuan Zhang[a]

Received 4th December 2023
Accepted 1st February 2024

DOI: 10.1039/d3ra08266k

rsc.li/rsc-advances

By employing the radical polymerization method, acrylonitrile (AN) was grafted on the surface of nano titanium dioxide ($TiO_2$), and the calcium sulfate whisker (CSW) was modified using the coupling agent KH570 to provide ultraviolet (UV)-absorption capacity. The prepared $TiO_2$-PAN and CSW-PAN materials can improve the anti-aging performance and mechanical properties of polypropylene (PP) and meet the application requirements of high-performance polypropylene. Further, the obtained PP composites show prolonged service life and application scope, which can effectively reduce white waste and avoid both resource waste and environmental pollution.

## Introduction

Polypropylene (PP) is a thermoplastic synthetic resin that has numerous advantages, such as chemical corrosion resistance, ease of processing, and excellent mechanical properties. This material is used in various fields of production and processing.[1–3] However, PP contains H atoms bonded to tertiary C, which are prone to breakage and oxidation under ultraviolet radiation, heat, and oxygen exposure, leading to a significant reduction in performance and shortened lifespan of PP products.[4–6] To improve the aging resistance of PP, researchers have developed organic,[7] inorganic,[8,9] and composite[10–12] ultraviolet (UV) absorbers. However, the problem of poor mechanical properties of small-molecule UV absorbers and their compatibility with high-molecular-weight polypropylene remain unsolved.[13,14] Therefore, it is necessary to develop a new type of polypropylene anti-aging agent that can enhance the aging resistance of PP without affecting its inherent excellent performance. This will help extend the service life of PP and ensure good system compatibility, thereby avoiding waste and environmental pollution.

Nano $TiO_2$ (titanium dioxide) has the ability to shield against UV radiation. However, due to the presence of numerous hydroxyl groups on its surface, it tends to aggregate and does not disperse well. To overcome this issue, silane coupling agents are usually used to modify the surface. These agents are chemically bonded to the coupling molecules and wrapped around the surface of the titanium dioxide particles, improving their dispersion properties.[15–17] The resultant nano-titanium dioxide is still a small-molecule material and cannot coexist with PP for a long time. Acrylonitrile (AN) also has UV-shielding ability and can achieve the dual role of anti-aging when grafted on $TiO_2$, but it cannot fundamentally improve the performance of PP, and the prepared polypropylene material cannot be used in specific engineering fields and high-performance polypropylene products. Calcium sulfate whisker (CSW), an economical and effective toughening agent, is often used to improve the poor compatibility and mechanical properties of polymers.[18–20] CSW has high strength and high modulus, which make it a popular choice for developing enhanced and modified polymer materials.[21–23] The surface of CSW can be modified with a coupling agent to make it organic,[24,25] thus improving its compatibility with polymer materials.[26–28] When acrylonitrile is grafted onto CSW, it can also partially absorb UV light due to the presence of the –CN group.

In this study, we grafted acrylonitrile on the surface of a calcium sulfate whisker so that it can improve the mechanical properties while also shielding part of the ultraviolet-light. The addition of a calcium sulfate whisker improved the dispersion of $TiO_2$ in the PP matrix, achieving enhanced UV-shielding function. The mechanical test results showed that only 3% content of $TiO_2$-PAN and CSW-PAN particles could effectively improve the mechanical properties of the fabricated polypropylene products. Atomic force microscopy and scanning electron microscopy proved that their dispersion in the polypropylene materials was significantly improved. Herein, the prepared new anti-aging agents $TiO_2$-PAN and CSW-PAN are expected to provide technical reserve for the production of new

[a]School of Chemistry and Chemical Engineering, Qiaihar University, Qiaihar, China
[b]College of Materials Science and Engineering, Qiaihar University, Qiaihar, China. E-mail: 409222743@qq.com
[c]Northeast Petroleum University Applied Technology Research Institute, Northeast Petroleum University, Daqing, China
[d]College of Materials Science and Engineering, Heilongjiang Province Key Laboratory of Polymeric Composition Material, Qiaihar University, Qiaihar 161006, China. E-mail: wyz6166@nefu.edu.cn

† Electronic supplementary information (ESI) available. See DOI: https://doi.org/10.1039/d3ra08266k

polypropylene materials. As the service life of these polypropylene materials is extended, white waste, resource waste, and environmental pollution can be reduced.

## Experimental methods

### Materials and apparatus

Rutile nano $TiO_2$ ($TiO_2$) was purchased from Xuancheng Jingrui New Materials Co., Ltd (Anhui, China). γ-Methylpropenoxy propyl tri-methoxysilane (KH570) was purchased from Nanjing Xiangqian Chemical Co., Ltd (Nanjing, China). Acrylonitrile (AN) was purchased from Tianjin Fuchen Chemical Reagent Factory Co., Ltd (Tianjin, China). Azodiisobutyronitrile (AIBN) was purchased from Shanghai Sihe Microchemical Co., Ltd (Shanghai, China). *N*,*N*-Dimethylformamide (DMF) was purchased from Shanghai Pharmaceutical Group Chemical Reagent Factory Co., Ltd (Shanghai, China). Acetone (AC) was purchased from Tianjin Quartz Clock Factory Bazhou Chemical Division Factor Co., Ltd (Tianjin, China). Sodium dodecyl benzene sulfonate (SDBS) was purchased from Sinopsin Chemical Reagent Co., Ltd (Shanghai, China). Polypropylene (PP industrial grade) was purchased from Daqing Huaoke Co., Ltd (Daqing, China). Calcium sulfate whiskers (CSW) were obtained from Shanghai Fengzhu Whisker Trading Co., Ltd (Shanghai, China). All chemicals were used as received.

Fourier transform infrared spectroscopy was used to characterize the characteristic peaks of the samples. The crystal structures of the samples were characterized using X-ray diffraction. The UV absorption properties of the samples were determined using UV-vis absorption spectroscopy. Sample aging was analyzed using an accelerated aging tester. A universal testing machine was used to test the mechanical properties of the samples. Dynamic rheometers were used to test the thermodynamic properties of the materials. Atomic force microscopy was used to analyze the interface of the composite materials. Scanning electron microscopy (SEM) was employed to test the aged interface.

### Preparation of $TiO_2$-PAN composite materials

To achieve pure intermediate KH570-$TiO_2$, a mixture of nano-titanium dioxide, anhydrous ethanol, and distilled water was prepared and placed in an ultrasonic cell pulverizer. The mixture was heated to 80 °C with stirring, and then a specific amount of acetic acid and KH570 were added. After three hours of reaction, the resulting KH570-$TiO_2$ was washed by centrifugation and dried. The KH570-$TiO_2$ was then mixed with SDBS, followed by the addition of anhydrous ethanol and distilled water for ultrasonic detection. The mixture was stirred and heated to 65 °C, and certain amounts of AN and AIBN were added. After eight hours of reaction, $TiO_2$-PAN was post-treated with DMF and AC. The reaction environment was maintained oxygen-free.

### Preparation of the CSW-PAN composite materials

To achieve the pure intermediate KH570-CSW, ultrasonic hydrolysis was performed, add 3% of the relative mass of KH570 to ethanol. CSW was then placed in an 80 °C water bath and stirred. The resulting product suspension was washed with ethanol and then allowed to settle and dry naturally to obtain KH570-CSW. Next, appropriate amounts of KH570-CSW and SDBS were weighed, mixed with anhydrous ethanol and distilled water, sonicated, stirred, and heated to 65 °C. Specific amounts of AN and AIBN were added and allowed to react for 8 hours. Initially, the product was washed with DMF and then rinsed with distilled water and AC. Finally, the suspension was dried to obtain CSW-PAN.

The reaction environment was maintained oxygen-free.

### Preparation of the $TiO_2$-PAN/CSW-PAN/PP composite materials

In this experiment, the amount of CSW-PAN added to the PP matrix was fixed at 3%, and on this basis, the amounts of $TiO_2$-PAN added were 1, 3, 5, and 7%, respectively. The $TiO_2$-PAN/PP, CSW-PAN/PP, and $TiO_2$-PAN/CSW-PAN/PP composite materials were mixed in different proportions uniformly using an internal mixer. The mixture was then used to create splines through injection molding. To compare with pure PP splines, we first predried the samples and prepared them to a standard size for testing impact, tensile, and bending. To obtain the PP composite material, we added 40 g of dried PP and the reactant in a certain proportion to the mixer at 180 °C to melt and blend. The resulting product was crushed with a small plastic crusher and then injected into the injection molding machine to produce dumbbell-shaped and round splines for testing.

### Sample characterization

The powder samples were characterized using Fourier transform infrared spectroscopy (FTIR), and the samples were scanned by infrared spectroscopy in a scanning range of 4000–500 $cm^{-1}$. An X-ray photoelectron spectrometer was used to characterize the structure of the samples. Test parameters: tube pressure 40 kV, tube flow 200 μA, Cu target, diffractive width DS = SS = 1°, RS = 0.3 mm, scan speed 2000 d $min^{-1}$, scan range 10–90°. UV-vis absorption spectroscopy was used to determine the UV absorption properties. An accelerated aging tester was employed to test for sample aging. The correlation coefficient of radiation intensity (0.89 W $m^{-2}$), blackboard temperature (63 ± 3 °C), relative humidity (65 ± 5%), spray cycle (18/102 min), and aging time (1000 h) were set to specific values. A universal testing machine was used to evaluate the mechanical properties. Each sample was tested six times, and the average values were considered. Dynamic rheometers were used for assessing the thermodynamic performance. During the test, the temperature was set to 230 °C, and the scanning frequency range was set to 0.01–100 rad $s^{-1}$. Interface analysis was performed using atomic force microscopy. The post-aging interface was analyzed using scanning electron microscopy. The surface of each sample was sprayed with gold to increase the electrical conductivity. The samples were placed in a vacuum chamber, and the morphologies of different samples were observed under an acceleration voltage of 9.5 kV.

## Results and discussion

### Characterization and analysis of $TiO_2$-PAN

In Fig. 1, the absorption peaks at 3434 $cm^{-1}$ and 1634 $cm^{-1}$ (caused by water absorption during the test) correspond to the hydroxyl group of water on the surface of $TiO_2$. The peak at 1717 $cm^{-1}$, 1621 $cm^{-1}$, and 1258 $cm^{-1}$ correspond to the C=O, C=C, and C–O–C bonds of KH570, while the peak at 904 $cm^{-1}$ corresponds to Ti–O–Si moiety generated from the reaction of KH570 and $TiO_2$, demonstrating the successful coating of KH570 on the $TiO_2$ surface. The peaks at 1189 $cm^{-1}$ and 1723 $cm^{-1}$ indicate the C–O–C and C=O stretching vibrations of KH570, while the peaks at 1453 $cm^{-1}$ and 2241 $cm^{-1}$ correspond to the stretching vibrations of C≡N, demonstrating the successful grafting of AN. The above analysis of the FTIR spectra confirms that the products KH570-$TiO_2$ and $TiO_2$-PAN were successfully obtained.[29,30]

In Fig. 2, the XRD spectrum shows pure $TiO_2$ nanoparticles. The characteristic peaks at 25.28°, 37.80°, 48.04°, 53.89°, 55.06°, and 62.68° correspond to the (101), (004), (200), (105), (211), and (204) crystal planes of rutile $TiO_2$ crystals, respectively (PDF# 21-1272). In comparison with KH570-$TiO_2$, the diffraction peak offset at 10–25° and the emergence of a new diffraction peak at 20.96° corresponding to C (PDF# 79-1715) in curve b prove the successful coating of KH570. The complete disappearance of the diffraction peak at 10–25° and the high-intensity diffraction peaks in curve c prove the successful grafting of acrylonitrile.

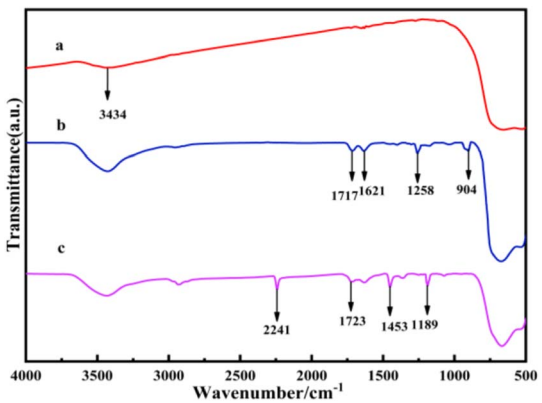


Fig. 1 FTIR spectra of unmodified and modified $TiO_2$: (a) $TiO_2$, (b) KH570-$TiO_2$ and (c) $TiO_2$-PAN.

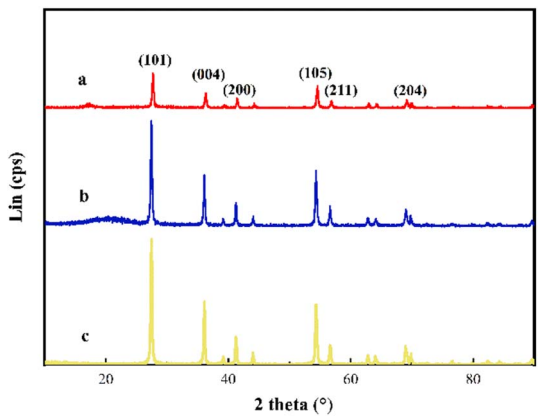


Fig. 2 XRD patterns of unmodified and modified $TiO_2$: (a) $TiO_2$, (b) KH570-$TiO_2$, and (c) $TiO_2$-PAN.

### Characterization and analysis of CSW-PAN

In Fig. 3, the difference in the CSW spectrum is evident after coating with the KH570 coupling agent and grafting with acrylonitrile. The OH telescopic peaks of CSW were observed at 3618 $cm^{-1}$ and 3560 $cm^{-1}$, while signals of the C=O and C–O–C bonds were seen, at 1117 $cm^{-1}$ and 1732 $cm^{-1}$, respectively. The reaction of KH570 with CSW generates Ca–O–Si, as evidenced by the peak at 958 $cm^{-1}$, proving the successful coating of KH570 on the CSW surface. The peak of S–O of CSW was not seen. The stretching vibration peaks of the CN triple bond were observed at 1453 $cm^{-1}$ and 2241 $cm^{-1}$, indicating that the carbon–carbon double bond of KH570 has reacted with the AN double bond. From the FTIR spectra analysis, it is evident that the products KH570-CSW and CSW-PAN were successfully obtained.

In Fig. 4, the XRD spectrum of pure CSW nanoparticles displays the characteristic peaks at $2\theta = 14.62°$, 25.50°, 29.31°, and 32.00°, which correspond to the (100), (110), (111), and (102) planes of anhydrous CSW crystals, respectively (PDF# 45-0157). As coating and grafting occur only on the surface of the whisker, the lattice structure and atomic arrangement inside the whisker would remain unchanged. Therefore, the characteristic peak of the crystal after coating and grafting did not undergo significant changes. This proves that KH570 modification and acrylonitrile grafting did not affect the crystal structure of anhydrous CSW.

### Analysis of the aging properties of the $TiO_2$-PAN/CSW-PAN/PP composites

In Fig. 5, the $TiO_2$/PP composites can absorb ultraviolet light in the 200–400 nm range. However, $TiO_2$ is highly polar and prone

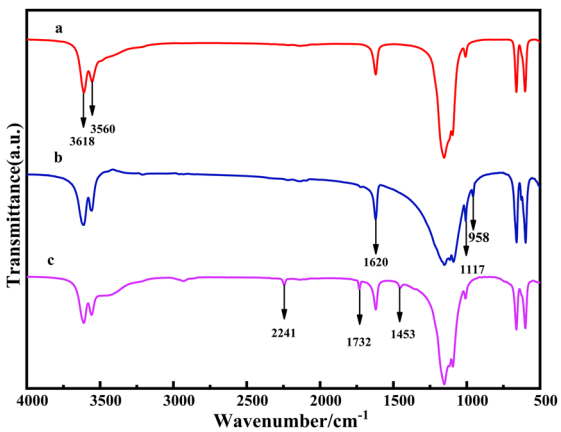


Fig. 3 FTIR spectra of unmodified and modified CSW: (a) CSW, (b) KH570-CSW, and (c) CSW-PAN.

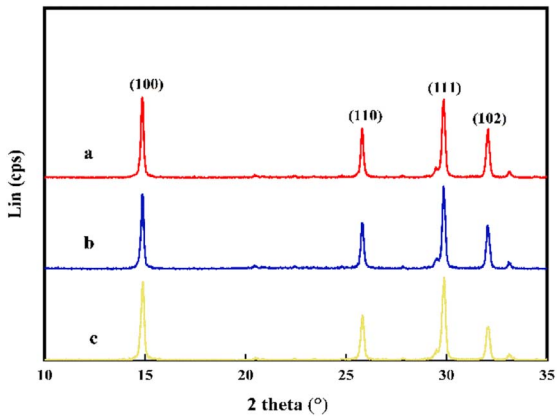


Fig. 4 XRD patterns of unmodified and modified CSW: (a) CSW, (b) KH570-CSW and (c) CSW-PAN.

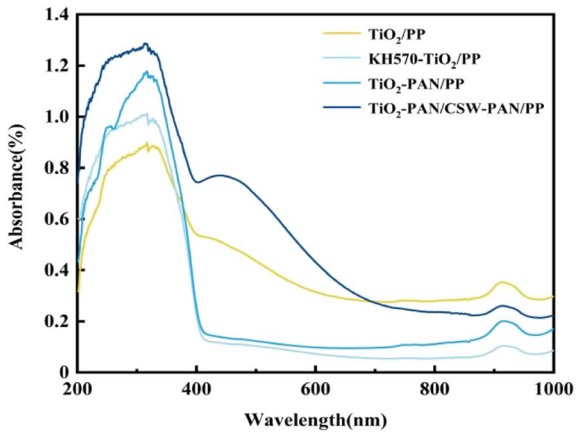


Fig. 5 UV-VIS spectrum of the $TiO_2$/PP composites.

to agglomeration, which negatively affects its dispersibility and anti-aging properties in the PP matrix, thereby limiting its ability to provide ultraviolet protection. When modified by the coupling agent KH570, the surface of $TiO_2$ undergoes organic modification, which enhances its compatibility and dispersion in PP, and increases the degree of ultraviolet light absorption. The absorption strength of the $TiO_2$-PAN/PP composites was greater than that of the $TiO_2$/PP and KH570-$TiO_2$/PP composites. This was due to the addition of PAN, which improved the UV resistance of PP through its UV shielding function. The noticeable and broad absorption peaks that are enhanced in the 200–400 nm and 400–500 nm ranges can be attributed to the higher level of UV absorption by $TiO_2$ in the $TiO_2$-PAN/CSW-PAN/PP after the addition of the crystal whiskers and the improved compatibility between $TiO_2$ and the PP matrix. This is also because both KH570-$TiO_2$ and KH570-CSW were grafted with PAN, which has a UV shielding effect. This imparted a double UV-shielding effect and improved UV absorption intensity. Generally, the UV absorption intensity of $TiO_2$-PAN/CSW-PAN/PP was significantly higher than that of $TiO_2$/PP and KH570-$TiO_2$/PP. Hence, $TiO_2$-PAN/PP could be used to enhance the anti-aging performance of PP.

In Fig. 6, the CSW/PP composites showed a poor ability to absorb UV in the range of 200–400 nm, and the composite modified by the silane coupling agent KH570 showed a slight increase in the UV absorption capacity. The application of the coupling agent KH570 on the whisker surface enhanced its polarity and reduced its hydrophilicity, leading to increased UV absorption. CSW-PAN/PP composites have higher absorption strength than the other two because of PAN grafting, which provides UV-shielding ability and improves the UV resistance of the CSW/PP composites. This resulted in improved UV resistance of the CSW/PP composites. In the 200–400 and 400–500 nm ranges, $TiO_2$-PAN/CSW-PAN/PP exhibited broad absorption peaks. This is likely due to PAN grafting on both KH570-$TiO_2$- and KH570-CSW, which provides UV-shielding effects. Overall, the UV absorption strengths of $TiO_2$-PAN/CSW-PAN/PP were significantly higher than those of CSW/PP, KH570-CSW/PP, and CSW-PAN/PP. This characteristic can be used to enhance the antiaging properties of PP.

From Fig. 7, it can be observed that the impact strength and flexural strength first increased and then decreased with the addition of $TiO_2$-PAN. When excessive $TiO_2$-PAN was added, it did not work in synergy with CSW-PAN toward toughening but instead led to an increase in Rockwell hardness (Table 1). The bending strength was the highest at 3% $TiO_2$-PAN and showed strong toughness at low levels, reaching approximately 1.5 times that of pure PP. In this study, the fillers used enhanced the bending strength of pure PP. None of the samples broke during the bending test, and using CSW-PAN helped disperse $TiO_2$-PAN more effectively in the PP matrix, increasing the interfacial force. However, the tensile strength of the composite material decreased after reaching its maximum value. Excessive $TiO_2$-PAN caused severe agglomeration, preventing CSW-PAN from regulating filling and inhibiting its local aggregation in the PP area. This leads to stress concentration points and a decrease in the tensile strength. When a certain amount of CSW-PAN was added, the number of stress concentration points increased significantly at a $TiO_2$-PAN addition rate of 1%, resulting in an increase in fracture elongation at the macro level. However, this effect reached its maximum at a $TiO_2$-PAN

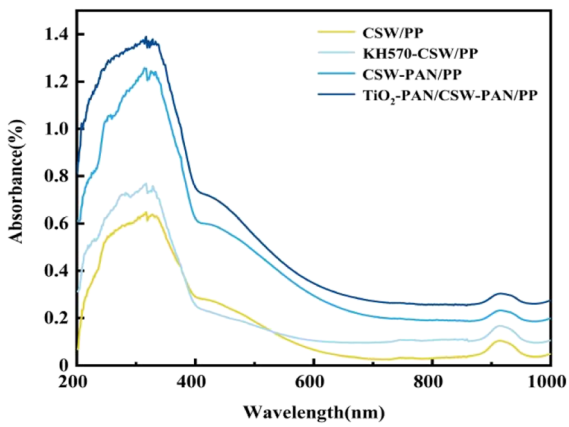


Fig. 6 UV-Vis spectrum of the CSW/PP composites.

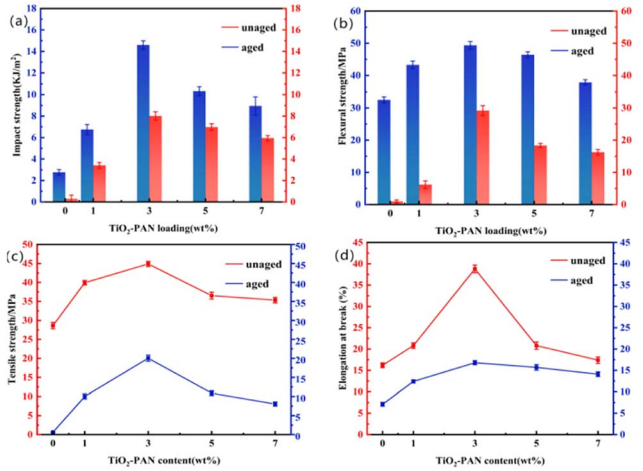


Fig. 7 Mechanical analysis of Impact Strength (a), flexural strength (b), tensile strength (c) and elongation at break (d) of PP and $TiO_2$-PAN/CSW-PAN/PP before and after aging.

content of 3%, and any further addition of $TiO_2$-PAN only suppressed interfacial compatibility and caused agglomeration.

After 1000 hours of aging, the mechanical properties of the material decreased. The impact strength and tensile strength of PP decreased by 10.42% and 2.98%, respectively, after aging. This suggests that PP was significantly degraded by UV light. However, when 5% of $TiO_2$-PAN was added, the impact strength retention rate remained high at 67.55%, and the best retention rate of bending strength at 3% addition was 59.08%. The tensile strength and fracture elongation of PP decreased to 0.62 MPa and 7.1%, respectively. However, when 3% $TiO_2$-PAN was added, the bending strength retention was 44.72%, indicating that $TiO_2$-PAN achieves double synergy with CSW-PAN. This reduces the aging degree of the material and effectively prevents the decline in mechanical properties. Therefore, the best performance was observed with 3% $TiO_2$-PAN. Compared with pure PP, these composite materials have higher retention rates, indicating their effective UV-shielding function.

### Dynamic mechanical properties

As shown in Fig. 8, the dynamic mechanical properties of poly($TiO_2$-PAN/CSW-PAN/PP) were analyzed using a dynamic

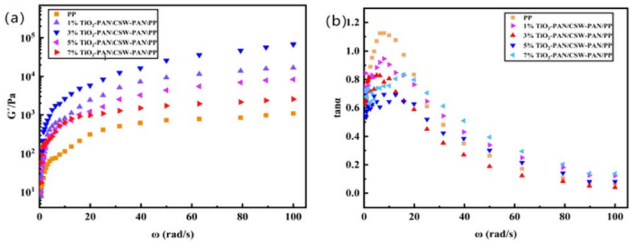


Fig. 8 Thermomechanical curves, storage modulus (a) and tan $\alpha$ (b), of PP and the $TiO_2$-PAN/CSW-PAN/PP composite materials.

mechanical performance tester. The trends of the energy storage modulus $G'$ and mechanical loss tan $\alpha$ are illustrated in the figure. In Fig. 8a, $G'$ is used to describe the elastic features of the composite materials, and it was observed that the $G'$ of all composites increased with an increase in $\omega$. In the low-frequency region, $\omega$ is smaller, and the cycle time given by $2\pi/\omega$ is much longer than the relaxation time of the molecular chain, so the polymer molecular chain segments have enough time to undergo rearrangement. With a continuous increase in $\omega$, the cycle time $2\pi/\omega$ is shortened below the relaxation time of the molecular chain, leading to incomplete rearrangement of the molecular chain segments and warranting the need to overcome intermolecular forces to do more work; therefore, $G'$ increases.

Mechanical loss is the ratio of $G''$ to $G'$ over a period of time. From Fig. 8b, it can be seen that the composites showed the pattern of an initial increase and then a decrease in this ratio with the increase in $\omega$. When the $\omega$ value is low, the chain segment movement inside the polymer is consistent with the external force, resulting in a low tan $\alpha$ value. However, as the $\omega$ value increases, more energy is consumed to overcome the friction resistance and change the conformation of the chain segment, causing an internal friction peak. The internal friction peak in the low-frequency region indicates that the contribution of the viscous response of the system is higher than that of the elastic response. As the value of $\omega$ increases further, the kinetic energy of the chain segment also increases. This results in a decrease in resistance to molecular motion, which is reflected by a decrease in the tan $\alpha$ value. The introduction of $TiO_2$-PAN has an impact on the dissipation factor of PP composites. As $\omega$ increases, the tan $\alpha$ values of the composites gradually surpass that of pure PP, eventually decline and tend to approach this value.

Table 1 Mechanical properties of the different composites

| Materials | Impact strength (kJ cm$^{-2}$) | Bending strength (MPa) | Tensile strength (MPa) |
|---|---|---|---|
| 1% $TiO_2$-PAN/PP | 3.062 | 40.838 | 35.12 |
| 3% $TiO_2$-PAN/PP | 3.973 | 44.322 | 38.51 |
| 5% $TiO_2$-PAN/PP | 3.554 | 41.67 | 36.89 |
| 7% $TiO_2$-PAN/PP | 3.4 | 39.399 | 35.71 |
| 1% CSW-PAN/PP | 5.186 | 44.404 | 38.92 |
| 3% CSW-PAN/PP | 12.462 | 46.838 | 41.15 |
| 5% CSW-PAN/PP | 9.973 | 44.476 | 39.47 |
| 7% CSW-PAN/PP | 7.106 | 39.2 | 38.33 |

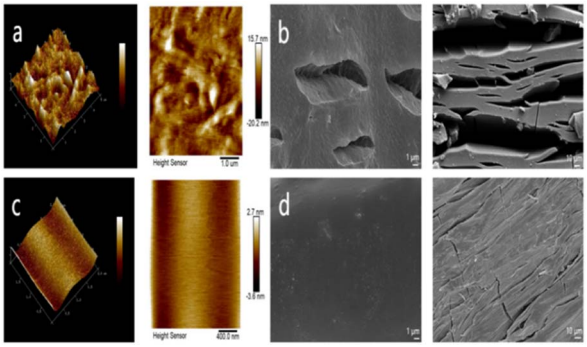


Fig. 9 Atomic force microscopy (AFM) analysis (a and c) and scanning electron microscopy analysis of the fracture surfaces after aging for 1000 hours (b and d).

**Analysis of the impact of the interface on aging performance**

Fig. 9 demonstrates that the degree of fusion of materials within the matrix of the composite $TiO_2$-PAN/CSW-PAN/PP is better than that of pure PP, whereas the roughness of $TiO_2$-PAN/CSW-PAN/PP is lower than that of PP according to Gwyddion calculations. The height phase diagram in Fig. 9a shows much higher ridges than those in Fig. 9c. The grooves and hills in the three-dimensional phase diagram prove that the pure PP surface was not smooth, the fracture surface has obvious cracks, and the surface was damaged after aging, which justifies the significantly reduced PP performance after aging (Fig. 9b). However, $TiO_2$-PAN/CSW-PAN/PP with good interfacial compatibility did not show obvious cracks after 1000 h of aging (Fig. 9c), which demonstrates that the presence of CSW-PAN makes the interface very strong (Fig. S1†). The impact performance of the corresponding composite material is better than that of unaged PP since the presence of CSW-PAN inhibits the aggregation of $TiO_2$-PAN in PP and improves its distribution, thereby enhancing its binding force at the interfaces and allowing $TiO_2$-PAN to exhibit UV shielding to its full potential. At the same time, CSW-PAN can also absorb weak UV light, so cracks occur only on the surface of the PP fibers; thus, its mechanical properties are not significantly reduced under long UV exposure.

## Conclusions

Compared with pure PP, the anti-aging properties of the $TiO_2$-PAN/CSW-PAN/PP ternary composites were improved. $TiO_2$-PAN enhances the UV shielding ability of PP, whereas, CSW-PAN plays a role in toughening the material. When CSW-PAN and $TiO_2$-PAN were combined in the correct proportion, they could work together to enhance the mechanical properties of the PP matrix. Nevertheless, too much $TiO_2$-PAN led to a notable decrease in performance. This is because a large amount of $TiO_2$-PAN cannot be evenly dispersed under the influence of CSW-PAN, resulting in the formation of numerous aggregates. The atomic force microscopy results prove that CSW-PAN effectively improves the dispersion and interface binding force of $TiO_2$-PAN in the PP collective. Combined with the observations from scanning electron microscopy and mechanical performance tests, our findings prove that this composite polypropylene material displays effectively improved anti-aging performance and meets the practical application requirements of high-performance polypropylene, and therefore, has the potential to effectively extend the service life of commodities and avoid unnecessary waste and white pollution.

## Conflicts of interest

There are no conflicts to declare.

## Acknowledgements

This work was supported by the Key Project Tasks of the Science and Technology Plan in Qiqihar City (ZDGG—202302).

## References

1 Hemlata, *Polym. Compos.*, 2023, **44**(9), 5409–5432.
2 A. A. Yousefi, *Polym. Compos.*, 2023, **44**, 5464–5479.
3 H. H. Zhu, W. H. Wang, Y. Wang, Z. B. Lin, H. J. Ji, X. Chen, G. Li, Y. L. Ma and L. S. Xie, *Polym. Compos.*, 2023, **44**, 5553–5566.
4 S. R. Karanjikar and S. S. Lakade, *Mater. Today*, 2022, **50**, 1644–1652.
5 M. Atagur, Y. Seki, Y. Pasaoglu, K. Sever, Y. Seki, M. Sarikanat and L. Altay, *Polym. Compos.*, 2020, **41**, 1–11.
6 J. H. Zhao, X. Liu, R. Yang and J. Yu, *J. Appl. Polym. Sci.*, 2015, **132**, 42546.
7 Y. Taguchi, Y. Ishida, H. Ohtani and H. Matsubara, *Anal. Chem.*, 2004, **76**, 697–703.
8 S. Morlattherias, B. Mailhot, D. Gonzalez and J. Gardette, *Chem. Mater.*, 2005, **17**, 1072–1078.
9 E. P. d. Nascimento, C. B. B. Luna, E. d. S. B. Ferreira, E. A. d. S. Filho, D. D. Siqueira, R. M. R. Wellen and E. M. Araújo, *Polym. Compos.*, 2023, **44**, 5891–5909.
10 Y. Liu, Y. J. Guan, J. Q. Zhai, F. J. Chen, H. Q. Chu, G. F. Hu and J. Lin, *Polym. Compos.*, 2023, **44**, 6228–6241.
11 A. K. Maurya, R. Mahadeva, G. Manik and S. P. Patole, *Polym. Compos.*, 2023, **44**, 5104–5120.
12 K. J. Singala, A. A. Mungray and A. K. Mungray, *Ind. Eng. Chem. Res.*, 2012, **51**, 10557–10564.
13 S. M. Khaled, R. H. Sui, P. A. Charpentier and A. S. Rizkalla, *Langmuir*, 2007, **23**, 3988–3995.
14 B. Xiang, G. Jiang and J. Zhang, *Plast., Rubber Compos.*, 2015, **44**, 148–154.
15 H. Zhang, F. Li and H. Zhu, *Fibers Polym.*, 2013, **14**, 43–51.
16 M. Sabzi, S. M. Mirabedini, J. Zohuriaan-Mehr and M. Atai, *Prog. Org. Coat.*, 2009, **65**, 222–228.
17 G. Guo, Q. W. Shi, Y. B. Luo, R. R. Fan, L. X. Zhou, Z. Y. Qian and J. Yu, *Nanoscale Res. Lett.*, 2014, **9**, 215.
18 G. H. Xiang, T. Liu, Y. M. Zhang and N. N. Xue, *Results Phys.*, 2018, **10**, 28–35.
19 B. He, X. F. Lin and Y. F. Zhang, *J. Therm. Anal. Calorim.*, 2018, **132**, 1145–1152.
20 J. C. Wang, L. J. Tang, D. Wu, X. Guo and W. L. Hao, *Polym. Polym. Compos.*, 2012, **20**, 453–462.

21 J. N. Yang and S. B. Nie, *Polym. Degrad. Stab.*, 2017, **144**, 270–280.
22 Q. Dou and Ji. W. Duan, *Polym. Compos.*, 2016, **37**, 2121–2132.
23 W. J. Yuan, J. Y. Cui, Y. B. Cai and S. A. Xu, *J. Polym. Res.*, 2015, **22**, 173.
24 W. J. Yuan, J. Y. Cui and S. A. Xu, *J. Mater. Sci. Technol.*, 2016, **32**, 1352–1360.
25 J. Wang, K. Yang and S. Lu, *High Perform. Polym.*, 2011, **23**, 141–150.
26 D. H. Zhu, X. Y. Nai, S. J. LanS, J. Bian, X. Liu and W. Li, *Appl. Surf. Sci.*, 2016, **390**, 25–30.
27 Y. Chen, Y. Ding, Y. J. Dong, Y. T. Liu, X. Ren, B. Wang and C. H. Gao, *J. Polym. Sci.*, 2020, **58**, 624–635.
28 J. Wang, K. Yang and S. Lu, *High Perform. Polym.*, 2011, **23**, 141–150.
29 S. Mishra, M. Misra, S. S. Tripathy, S. K. Nayak and A. K. Mohanty, *Macromol. Mater. Eng.*, 2001, **286**, 107–113.
30 A. Nasir, A. Raza, M. Tahir and T. Yasin, *Mater. Chem. Phys.*, 2020, **246**, 122807.